International Journal of Thermofluids 22 (2024) 100713

Contents lists available at ScienceDirect

International Journal of Thermofluids

journal homepage: www.sciencedirect.com/journal/international-journal-of-thermofluids

MHD mixed convection of nanofluid flow Ag- Mgo/water in a channel contain a rotational cylinder

Falah A. Abood [a], Zainab K. Radhi [a], Ali K. Hadi [a], Raad Z. Homod [b,*], Hayder I. Mohammed [c]

[a] Mechanical Engineering Department, Basrah University, Basra, Iraq
[b] Department of Oil and Gas Engineering, Basrah University for Oil and Gas, Basra, Iraq
[c] Department of Cooling and Air Conditioning Engineering, Imam Ja'afar Al-Sadiq University, Baghdad, Iraq

ARTICLE INFO

Keywords:
Mixed flow
Horizontal channel with triangular cavity
Hybrid nanofluid

ABSTRACT

This investigation explores the mixed convection phenomenon of a hybrid nanofluid flowing within a Channel oriented horizontally featuring a triangular cavity attached to the lower channel wall. The cavity houses a rotating circular cylinder with a radius of R = 0.12. The fluid within the enclosure is a water-based nanofluid containing Ag-MgO nanoparticles. Two scenarios of combined natural and forced convection are examined: in Case 1, all channel walls, the left wall of the cavity, and the surface of the rotating cylinder are adiabatic, while the inclined wall of the cavity is isothermal. In Case 2, all channel walls, the ready wall of the cavity, and the surface of the rotating cylinder are adiabatic, except for the left wall of the cavity, which is isothermal. The dimensionless governing equations are solved under steady flow conditions for various physical parameters using a higher-order and stable Galerkin-based finite element method implemented through the software package FlexPDE. Key governing parameters such as Re number (falling within the amplitude of 10 to 100), Ri number (ranging from Ri = 0.1 to 30), and the location of cylinder rotation (Xo = 0.65 to 0.9) are simulated. The study presents results in terms of average Nusselt numbers and contour maps of streamlines and isotherms. It is observed that the average Nusselt number increases with higher Reynolds number, angular rotation speed, cylinder location, and Richardson number. Specifically, heating the inclined surface suggests that the optimal location for the rotating cylinder is Xo = 0.9, whereas if the left wall of the cavity is heated, the preferred location for the cylinder is Xo = 0.75. These findings are corroborated by comparing them with previous research, demonstrating significant agreement.

1. Introduction

Mixed convection and heat transfer occurring within cavities represent a significant phenomenon in both scientific and engineering realms, owing to their wide applicability across various systems such as photovoltaic panels, technologies of extracting moisture from substances, and performance insulation by minimizing heat transfer, etc. Over the past decades, considerable attention has been directed towards understanding the flow structure and heat transfer characteristics associated with fluid flow over open cavities, given their critical role in diverse engineering applications across different scales. This geometric configuration finds application in cooling electronic components at small scales, while at medium scales, it is employed in solar collectors equipped with wind barriers. Beyond these applications, the primary reason for the keen interest in this geometry lies in its frequent utilization in the simplest isothermal configuration to validate computational models and numerical codes. Several studies have investigated mixed convection flows in cavities with a spinning circular cylinder placed at different positions [1–5].

Nanofluids have recently garnered considerable interest as potential cooling agents in various industrial applications, leading to a rise in research endeavors to thoroughly investigate their thermal efficiency. Suchana et al. [6] studied natural convection cooling in an enclosed space filled with nanofluids. Their investigation notably examined a heat source on the bottom wall while lowering the temperatures on the other walls. The main factors considered were the influence of Rayleigh number, heat source position, shape, type of nanofluid, and the proportion of solid nanoparticles on cooling effectiveness. Adding nanoparticles to clean water significantly improved its cooling effectiveness, especially when the Rayleigh numbers were low.

Al Kalbani et al. [7] provided significant knowledge by reporting

* Corresponding author.
E-mail address: raadahmood@yahoo.com (R.Z. Homod).

https://doi.org/10.1016/j.ijft.2024.100713

Available online 27 May 2024

Nomenclature

Gr	Grashof number
g	Acceleration (m/s^2)
L	Length
Nu	Average Nusselt number
Pr	Prandtl number
R	The dimensional radius of the cylinder
Ra	Rayleigh number
Re	Reynolds number
Ri	Richardson number
Ha	Hartmann number
T	Temperature (K)
T_h	Elevated temperature (K)
u,v	Components of velocity (m/s)
X, Y	Coordinates x, y
K	Fluid conductivity (W m^{-1} K^{-1})
P	Pressure (N m^{-2})
Cp	Air Specific heat of the air (J kg^{-1} K^{-1})
$T_{.C.}$	Low Temperature (K)
B	Density of Magnetic flux (Wb)

Greek symbols

α	Diffusivity (m^2/s)
β	Expansion coefficient (1/K)
υ	Kinematic viscosity (m^2/s)
ρ	Fluid density (kg/m^3)
Ω	Dimensionless angular velocity
μ	Dynamic viscosity (kg/m.s)
θ	Dimensionless temperature
α	Electrical conductivity effective $(\Omega m)^{-1}$
ϕ	Fraction volume
ω	Dimensional Angular velocity (rad/*sec*)
β	Coefficient of thermal expansion (1/K)

quantitative findings for the movement of nanofluids within a square enclosure. Their research investigated the impact of solid volume percentage on mixed convection flows, offering a detailed comprehension of the interaction between these factors. Saleh et al. [8] expanded their investigation to include the study of natural convection heat transport in a trapezoidal cage filled with a nanofluid. Their studies highlighted that the presence of steep walls and high concentrations of Cu nanoparticles significantly increased heat transfer rates in the system. Abbasian et al. [9] conducted a numerical study on the laminar flow of a mixture of convection around a non-heating object in a container driven by a lid filled with a nanofluid. This study examined the effects of varying thermal conductivity and viscosity, providing new insights into the complex dynamics of mixed convection.

Mahmoodi and Hashemi [10] investigated the phenomenon of natural convection fluid flow and heat transfer in C-shaped shells filled with copper and water nanofluids. Their study investigated the impact of Rayleigh number and copper nanoparticle volume percentage on heat transmission, contributing to a deeper knowledge of nanofluid behavior in specific geometric arrangements. Izadi et al. [11] performed a thorough examination, categorizing research on the combined convection of nanofluids in enclosed spaces according to their geometric arrangements. Uysal and Korkmaz [12] investigated the convective heat transfer and entropy production properties of Ag-MgO nanoparticles dispersed in water, flowing via rectangular mini channels. Their study provided valuable information on the performance of these arrangements.

In their study, Hasan et al. [13] investigated the flow of a mixed nanofluid in a lid-driven cavity under the influence of natural convection. They specifically focused on the flow behavior when a thick conductive solid layer is above the heated wall. In their study, Hussain et al. [14] examined the impact of a permeable layer on the flow dynamics, heat transfer, and hydrodynamic forces of a hybrid nanofluid in a channel including an exposed hollow. Ahmadianfar [15] conducted experimental and numerical research to examine the impact of laminar separation flow and nanofluids on heat transmission. The study focused on passive strategies, such as using ribs on walls and alterations in cross-sectional area. Chamkha and Selimefendigil [16] investigated the forced convection of pulsating nanofluid flow over a backward-facing step, considering different particle morphologies.

Lee et al. [17] conducted an experimental study to assess the thermal conductivity of nanofluids made of Al2O3 water and copper water. The study highlighted the observed pattern of rising thermal conductivity with a higher solid volume percentage. In their research, Khanafer et al. [18] conducted a computational analysis of the natural convection of a nanofluid consisting of copper nanoparticles dispersed in water within a two-dimensional enclosure. Their study uncovered a relationship between heat transfer and the concentration of copper nanoparticles in the fluid. In their research, Ali et al. [19] conducted a numerical simulation to analyze the phenomenon of buoyancy-driven convection in an enclosed space filled with a nanofluid consisting of Al-water. Santra et al. [20] conducted a numerical study on the heat transfer caused by natural convection that occurred within a square enclosure, which was differentially heated and contained a nanofluid comprising copper and water. In addition, several more studies [21–25] have conducted simulations of natural convection heat transfer employing nanofluids in different geometric shapes. The thermal conductivity of nanofluids has been determined using a model developed by Patel [26]. Saha et al. [27] examined how the size and placement of an obstruction affect buoyancy driven by convection within a Concentric ring-shaped region. In this configuration, the inner cylinder of the annulus was kept at an elevated temperature than the external cylinder. The primary discovery was to demonstrate that the mean heat rate significantly enhances until a specific size of the block and the type of convection regime. However, beyond this threshold, there is a deterioration in thermal behavior. Saha et al. [28] Explored the heating or cooling efficacy of convective thermal systems and demonstrated that it is heavily reliant on their geometrical shapes and configurations, alongside other controlling factors.

Biswas et al. [29] Their goal was to investigate the combined thermo-bioconvection phenomenon involving a magnetically responsive fluid comprising copper nanoparticles and oxytactic bacteria within a unique W-shaped permeable enclosure. Mandal et al. [30] In their study, they have endeavored to numerically investigate the thermo-fluidic transport phenomenon within an innovative M-shaped enclosure filled with permeable material, wherein Al_2O_3–Cu hybrid nanoparticles are suspended in water, all subjected to the influence of a horizontal magnetizing field. Manna et al. [31] study aimed to systematically evaluate the effects of the heater and cooler positions by utilizing four distinct quadrant-shaped recesses containing a hybrid nanofluid while maintaining the adiabatic curved surface under oriented magnetic fields. They conducted analyzing both heat transfer and entropy generation for the flow of a hybrid nanofluid within a quarter circular channel while considering different arrangements of magnetic fields.

This study explores the heat transfer mechanisms in a two-dimensional channel configuration with a triangular cavity at its base containing a rotating cylinder using a hybrid nanofluid influenced by a magnetic field. Two configurations are examined: one with insulated walls except for the vertical wall of the triangular cavity and the other with insulation on all walls except the inclined surface of the cavity. The nanofluid used is a solution of water with Ag-MgO nanoparticles. The

Galerkin-based finite element method is employed to solve the governing equations. This research uniquely investigates various factors such as angular velocity, Reynolds (Re), and Richardson (Ri) numbers, aiming to enhance understanding of complex heat transfer phenomena in different geometries and operational conditions. Section 4 of the study thoroughly elucidates the process, parameters, and their impact on flow and heat transfer within the cavity, contributing to advancements in technologies involving magnetic fields and hybrid nanofluids. This study uniquely combines a rotating cylinder, magnetic field, and hybrid nanofluid in a triangular cavity to analyze heat transfer across various geometries and conditions (Re, Ri, angular velocity). This comprehensive approach offers deeper insights for future advancements.

2. Problem discribation

2.1. The physical configuration

The study includes a schematic diagram, shown in Fig. 1, illustrating the investigated system. The setup consists of a triangular hollow attached to the lower wall of an open-topped channel. The channel is filled with a hybrid nanofluid made of Ag-MgO water with Re number of 10 to 100 and Ri number of 0.1 to 30. A cylindrical structure cylinder is positioned strategically inside the canal. The work methodically examines two unique boundary conditions.

Case 1: In this scenario, all surfaces of both the cavity and the channel are presumed to be insulated, with the exception of the inclined surface of the cavity, which is designated as hot section, while the inlet at the left end remains maintained at a lower temperature. Case 2: Conversely, in this case, all walls of both the cavity and the channel are regarded as insulated, with the exception of the left wall of the cavity, which is designated as a hot wall, while the inlet at the left end remains maintained at a lower temperature. The hybrid nanofluid under investigation is treated as incompressible and Newtonian. The flow setup is presumed to be a two-dimensional (2D) configuration, laminar and steady. Effects such as heat radiation and viscosity in the governing equation are disregarded. Additionally, a magnetic field is applied at an angle γ and with a strength of B0, inclined to the surface, while the Joule heating effect associated with the magnetic field is disregarded. Fluctuations in density are accounted for using the widely accepted Boussinesq approximation.

2.2. The dimensionless governing model

The present study investigates two-dimensional, laminar mixed convection phenomena within an incompressible, Newtonian hybrid nanofluid. Notably, the effects of thermal radiation and viscous dissipation have been deliberately omitted in the energy equation. Additionally, thermal equilibrium is assumed between the nanoparticles and the base fluid. Thus, based on these specified assumptions, the governing equations for the fluid become as described in [37]. This deliberate simplification of the model allows for a focused exploration of the core dynamics associated with mixed convection in the context of the hybrid nanofluid system under consideration.

$$\frac{\partial u}{\partial x}+\frac{\partial v}{\partial y}=0 \tag{1}$$

$$u\frac{\partial u}{\partial x}+v\frac{\partial u}{\partial y}=-\frac{1}{\rho_{hnf}}\frac{\partial p}{\partial x}+\frac{\mu_{hnf}}{\rho_{hnf}}\left(\frac{\partial^2 u}{\partial x^2}+\frac{\partial^2 u}{\partial y^2}\right)+\frac{\sigma_{nf}B_o^2}{\rho_{nf}}\left(v\,sin\gamma cos\gamma-u\,sin^2\gamma\right) \tag{2}$$

$$u\frac{\partial v}{\partial x}+v\frac{\partial v}{\partial y}=-\frac{1}{\rho_{hnf}}\frac{\partial p}{\partial y}+\frac{\mu_{hnf}}{\rho_{hnf}}\left(\frac{\partial^2 v}{\partial x^2}+\frac{\partial^2 v}{\partial y^2}\right)+\frac{\sigma_{nf}B_o^2}{\rho_{nf}}\left(u\,sin\gamma cos\gamma-v\,cos^2\gamma\right)+\frac{(\rho\beta)_{hnf}}{\rho_{hnf}}g(T-T_c) \tag{3}$$

$$u\frac{\partial T}{\partial x}+v\frac{\partial T}{\partial y}=\alpha_{hnf}\left(\frac{\partial^2 T}{\partial x^2}+\frac{\partial^2 T}{\partial y^2}\right) \tag{4}$$

These equations form a system of partial differential equations governing fluid flow and temperature distribution in a two-dimensional domain. Eq. (1) represents continuity, ensuring mass conservation. Eqs. (2) and (3) are the components along the x and y directions of the Navier-Stokes equations, describing momentum conservation with terms for convective acceleration, pressure gradient, viscous forces, and additional effects like surface tension and buoyancy. Eq. (4) represents the conservation of energy, describing temperature changes due to conduction and convective heat transfer. These equations are fundamental in fluid mechanics and heat transfer analysis, enabling the understanding and simulation of various engineering phenomena.

Where $\mu_{hnf}$is the viscosity of hybrid nanofluid, ρ_{hnf} is the density of hybrid nanofluid, and γ is the angle of the magnetic field

The boundary conditions are given as:

- At the entrance or inlet:

$$u = u(y),\ v = 0,\ T = Tc$$

- At the exit or outlet :

$$\partial u/\partial x = \partial v/\partial x = \partial T/\partial x = 0$$

- At all boundaries of the channel and cavity, except for the heated cavity walls:

$$u = 0,\ v = 0,\ \partial\theta/\partial n = 0$$

- At the bottom or right cavity wall:

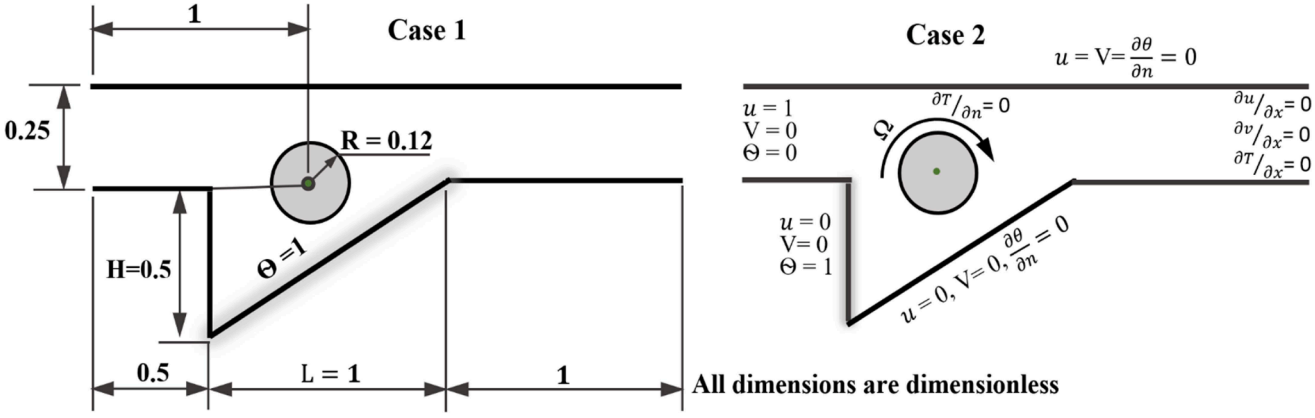

Fig. 1. A schematic geometry of the physical model.

$u = 0,\ v = 0,\ T = Th$

● At the boundary of the cylinder:

$u = -\omega(y - yo),\ v = \omega(x - xo),\ \partial T/\partial n = 0$

where ω is the angular speed.

2.3. The thermo physical properties

The effective properties of the hybrid nanofluid include properties such as density, thermal expansion coefficient, and heat capacity [33, 34].

$$\rho_{hnf} = (1-\varphi_{hnf})\rho_f + \varphi_{Ag}\rho_{Ag} + \varphi_{Mgo}\rho_{MgO} \tag{5}$$

$$(\rho\beta)_{hnf} = (1-\varphi_{hnf})(\rho\beta)_f + \varphi_{Ag}(\rho\beta)_{Ag} + \varphi_{Mgo}(\rho\beta)_{MgO} \tag{6}$$

$$(\rho C_p)_{hnf} = (1-\varphi_{hnf})(\rho C_p)_f + \varphi_{Ag}(\rho C_p)_{Ag} + \varphi_{Mgo}(\rho C_p)_{MgO} \tag{7}$$

Where the volume fraction of nanoparticles φ_{hnf} involving the two specified nanoparticles is provided as:

$$\varphi_{hnf} = \varphi_{Ag} + \varphi_{MgO} \tag{8}$$

The viscosity parameter of the hybrid nanofluid ($0 \le \varphi_{hnf} \le 0.02$) is determined as:

$$\frac{\mu_{hnf}}{\mu_f} = \left(1 + 32.795\varphi_{hnf} - 7214\varphi_{hnf}^2 + 714600\varphi_{hnf}^3 - 0.1941E8\varphi_{hnf}^4\right) \tag{9}$$

Where μ_f is the fluid viscosity.For this study, the thermal diffusivity and thermal conductivity of the hybrid nanofluid ($0 \le \varphi_{hnf} \le 0.02$) is presented by the following correlation relations, which are derived from experimental data [33,34], utilized for estimating the thermal conductivity and dynamic viscosity parameter of Ag-MgO/water hybrid nanofluid.

$$\alpha_{hnf} = \frac{\alpha_{hnf}}{(\rho C_p)_{hnf}} \tag{10}$$

$$\frac{K_{nhf}}{K_f} = \frac{(0.1747E5 + \varphi_{hnf})}{\left(0.1747E5 - 0.1498E6\varphi_{hnf} + 0.1117E7\varphi_{hnf}^2 + 0.1997E8\varphi_{hnf}^3\right)} \tag{11}$$

The Maxwell equation used for determining the effective electrical conductivity is expressed as [35].

$$\sigma_{hnf} = \sigma_f\left(\frac{1 + 3(\sigma_r - 1)\varphi_{hnf}}{(\sigma_r + 2) - (\sigma_r - 1)\varphi_{hnf}}\right) \tag{12}$$

where: $\sigma r = \sigma/\sigma f and \sigma = (\sigma Ag\varphi Ag + \sigma Mgo\varphi Mgo)/\varphi hnf$

Esfe et al. [29] conducted empirical experiments to establish connections for the nanoparticle volume fraction within $0 \le \varphi_{hnf} \le 0.03$ for the Ag-MgO/water hybrid nanofluid. Consequently, the derived practical connections are deemed valid within this specified range of nanoparticle volume fraction. The thermophysical characteristics of the individual components, namely MgO (40 nm), Ag (20 nm), and the base fluid (water), are elucidated in Ref. [28]. Notably, the hybrid nanoparticles in the numerical experiments consist of 50 % Ag, contributing to the hybrid nanofluid's overall composition in the investigated scenarios. These empirical connections and material characteristics provide a foundation for the subsequent numerical simulations and analyses in the context of the hybrid nanofluid system.

The thermal properties of Ag nanoparticles with a diameter of 20 nm, MgO nanoparticles with a diameter of 40 nm, and the host fluid water [35] are shown in Table 1.

The continuity, momentum, and energy equations are transformed from dimensional to dimensionless forms using the following variable conversions:

Table 1
The Ag and MgO properties.

Properties	Water	Ag	MgO
ρ(Kg/m^3)	997.1	10,500	3580
K (W/mK)	0.613	429	30
C_p(J/kg K)	4179	235	879
σ(1/Ωm)	0.05	6.3×10^7	1.42×10^{-3}
β(1/K)	21×10^{-5}	5.4×10^{-5}	33.6×10^{-6}

$$X = \frac{x}{L},\ Y = \frac{y}{L},\ U = \frac{u}{u_o},\ V = \frac{v}{u_o},\ \theta = \frac{T - T_c}{T_h - T_c}, P = \frac{p}{\rho_f u_o^2}$$

$$Re = \frac{u_o H}{\vartheta_f}, Gr = \frac{g\beta\Delta TH^3}{\vartheta_f^2},\ Pr = \frac{\vartheta_f}{\alpha_f},\ Ri = \frac{Gr}{Re^2},\ H_a = B_o H\sqrt{\frac{\alpha_f}{\mu_f}}$$

This transformation yields the following relations:

$$\frac{\partial U}{\partial X} + \frac{\partial V}{\partial Y} = 0 \tag{13}$$

$$U\frac{\partial U}{\partial X} + V\frac{\partial U}{\partial Y} = -\frac{\partial P}{\partial X} + \frac{1}{Re}\frac{\rho_f}{\rho_{hnf}}\frac{1}{(1-\varphi)^{2.5}}\left(\frac{\partial^2 U}{\partial X^2} + \frac{\partial^2 U}{\partial Y^2}\right) + \frac{\rho_f}{\rho_{nf}}\frac{\sigma_{nf}}{\sigma_f}\frac{Ha^2}{Re}\left(Vsin\gamma cos\gamma - Usin^2\gamma\right) \tag{14}$$

$$U\frac{\partial V}{\partial X} + V\frac{\partial V}{\partial Y} = -\frac{\partial P}{\partial Y} + \frac{1}{Re}\frac{\rho_f}{\rho_{hnf}}\frac{1}{(1-\varphi)^{2.5}}\left(\frac{\partial^2 V}{\partial X^2} + \frac{\partial^2 V}{\partial Y^2}\right) + \frac{\rho_f}{\rho_{nf}}\frac{\sigma_{nf}}{\sigma_f}\frac{Ha^2}{Re}\left(Usin\gamma cos\gamma - Vcos^2\gamma\right) + Ri\frac{\rho_f}{\rho_{hnf}}\left(1 - \varphi + \left[\frac{\varphi_{Ag}(\rho_s\beta_s)_{Ag} + \varphi_{Mgo(\rho_s\beta_s)_{Mgo}}}{\rho_f\beta_f}\right]\right)\theta \tag{15}$$

$$U\frac{\partial \theta}{\partial X} + V\frac{\partial \theta}{\partial Y} = \frac{\alpha_{hnf}}{\alpha_f}\frac{1}{RePr}\left(\frac{\partial^2\theta}{\partial X^2} + \frac{\partial^2\theta}{\partial Y^2}\right) \tag{16}$$

These equations represent the continuity, momentum, and energy equations transformed from dimensional form to dimensionless form using specific variable transformations. The transformed equations are expressed in terms of dimensionless variables such as U, V, θ, and P, where U and V represent velocity components, θ denotes temperature variation, and P signifies pressure. The dimensionless parameters Re, Gr, Pr, Ri, and Ha correspond to the Reynolds number, Grashof number, Prandtl number, Richardson number, and Hartmann number, respectively. These dimensionless equations describe fluid flow and heat transfer phenomena in a scaled domain, facilitating numerical analysis and solution without explicit dependence on system-specific dimensional parameters.

2.4. The boundary conditions

The physical boundary conditions in the dimensionless forms, used to solve Eqs. (13)–(16), are determined as:

- **At the inlet**

  $U = U(Y),\ V = 0,\ \theta = 0$ (For two cases)

- **At the outlet**

  $\partial U/\partial X = \partial V/\partial X = \partial\theta/\partial X = 0$ (For two cases)

- **For case 1**

  At all walls of the channel except the cavity-inclined wall

$U = 0,\ V = 0,\ \partial\theta/\partial n = 0$

At the inclined wall of the cavity

$U = 0,\ V = 0,\ \theta = 1$

- **For Case 2**

At all walls of the channel except the left side cavity

$U = 0,\ V = 0,\ \partial\theta/\partial n = 0$

At the left side of the cavity

$U = 0,\ V = 0,\ \theta = 1$

At the rotary cylinder

$U = \Omega(Y - Y\_o),\ V = -\Omega(X - X\_o),\ \partial\theta/\partial n = 0$

2.5. The Nusselt number

The local Nusselt number along the hot surface can be represented as:

$$Nu = \frac{k_{hnf}}{k_f}\left(\frac{\partial\theta}{\partial n}\right) \tag{17}$$

The average Nusselt number along the hot surface :

$$Nu_{avg} = \frac{1}{S}\int_0^S Nu\, dn \tag{18}$$

S represents the length of the hot surface, while n denotes the direction along the hot surface.

3. Computational methodology

3.1. Numerical scheme

The non-dimensional governing equations, coupled with the prescribed boundary conditions, were systematically solved through numerical techniques employing the Galerkin weighted residual method within the framework of the finite element method (FEM). The FlexPDE software was utilized for the analysis, specifically addressing the magnetohydrodynamics (MHD) mixed convection of the flow of the hybrid nanofluid. The studied configuration involves a triangular cavity affixed to the bottom wall of a horizontal channel with an open top, wherein an adiabatic circular cylinder is strategically positioned.

In the numerical solution domain, it is acknowledged that the set of Eqs. (13–16) may exhibit extreme oscillations or, in some instances, indeterminacy owing to the inclusion of the pressure term in the momentum equations. A derived approach within the finite element method is implemented to mitigate these challenges to stabilize pressure oscillations, allowing standard grids and elements to be used. This stabilization technique involves enforcing the continuity equation and pressure through a penalty approach, as detailed in [36]. This method enhances the numerical stability of the solution, ensuring reliable and accurate results in the investigation of the mixed convection of hybrid nanofluid flow within the specified geometric configuration.

$$\nabla^2 P = \lambda\left(\frac{\partial U}{\partial X} + \frac{\partial V}{\partial Y}\right) \tag{19}$$

The selection of λ values is typically guided by empirical knowledge or insights gained from prior studies. Commonly, a value of $\lambda = \frac{\mu}{L^2}$ is employed, as indicated in previous research [37], and this specific choice is adopted in the current formulation. Consequently, Eq. (13) becomes redundant in the computational process, and Eq. (19) is exclusively utilized instead of the former. This adjustment is made to enhance the numerical stability and efficiency of the solution, aligning with established practices in the field and contributing to the robustness of the model.

3.2. Work validation and numerical accuracy

3.2.1. Work validation

Software validation comprehensively examines grid dependency, continuity equation, and numerical results. This study systematically assesses grid dependency, and the continuity equation is rigorously validated for a particular grid resolution, guaranteeing accuracy to 10^{-4}. The mesh model utilized in the numerical simulation corresponds to specific parameters, including $\Omega = 5$, Ri = 1, $\varphi = 0.02$, $\alpha = 0$, Re = 10, $R = 0.12$, and Pr = 6.2. Fig. 2 provides a comprehensive depiction of the spatial distribution of the continuity equation ($\partial U/\partial X + \partial V/\partial Y$) across the entirety of the computational domain. This visualization is pivotal in our investigation as it serves as a visual representation of the meticulous validation process conducted to ensure the fidelity and precision of our numerical model. The solution is graphically depicted as a series of blue zigzag lines. These lines intersect the x-axis at various points, signifying that the corresponding equation evaluates to zero at those specific values. This is further corroborated by the accompanying numerical values presented alongside the figure. By presenting the validated continuity equation for the designated grid size, we establish a solid and reliable foundation for all subsequent analyses and interpretations concerning the mixed convection of hybrid nanofluid motion within the intricate geometric configuration under study. This validation process entails rigorous verification and comparison of computed values against analytical or experimental data, ensuring that our computational framework accurately captures the underlying physics of the flow phenomena. The modifications made to Fig. 2 include the incorporation of additional details and annotations aimed at providing further clarity and insight into the validation procedure, thereby enhancing the transparency and trustworthiness of our numerical simulations.

A comparative analysis was performed between the simulations carried out in this study and the stationary cylinder scenario described in Ref. [32]. Under particular conditions ($\Omega = 5$, Ri = 1, $\varphi = 0.01$, $R = 0.1$, Pr = 6.2, Re = 10), Fig. 3 compares the isotherms and streamlines between the current investigation and the work by Qureshi et al. [32]. As can be observed in Fig. 3a and b, respectively, the current program visualizes the results as lines, whereas Qureshi et al. [32] employ a color-based representation. This discrepancy arises from the differing software utilized in each investigation.

To mitigate concerns regarding this visual disparity, the average Nusselt number values obtained in this study were compared with those presented in Qureshi et al. [32] (Fig. 4). The close agreement observed in Fig. 4 serves as additional validation for the accuracy of the present results. The values of the average Nusselt number for the present study are simulated and compared in Table 2 with Ref. [32], which illustrates a good agreement.

3.2.2. Mesh independence study

Different types of Grids are selected for the refinement of mesh analysis. The deviations between Nusselt number results are minimal at large numbers of nodes and cells, as shown in Table 3. Therefore, the Grid that gives the result in less time is chosen throughout the simulation process. The mesh independence is represented in Fig. 5.

This study establishes the Nusselt number by identifying the minimum network size at which its value stabilizes. This value depends on several influencing factors, including the Rayleigh number (Ri), Reynolds number (Re), rotational speed, and direction of rotation. Fig. 5 exemplifies this approach. Here, the Nusselt number reaches a constant value (Nu= 3.902238) at a network size of 72,446 nodes. Further increases in network size do not produce any significant changes in the Nusselt number, as demonstrated in the figure. Therefore, this study adopts the verification approach presented in Fig. 5, selecting the

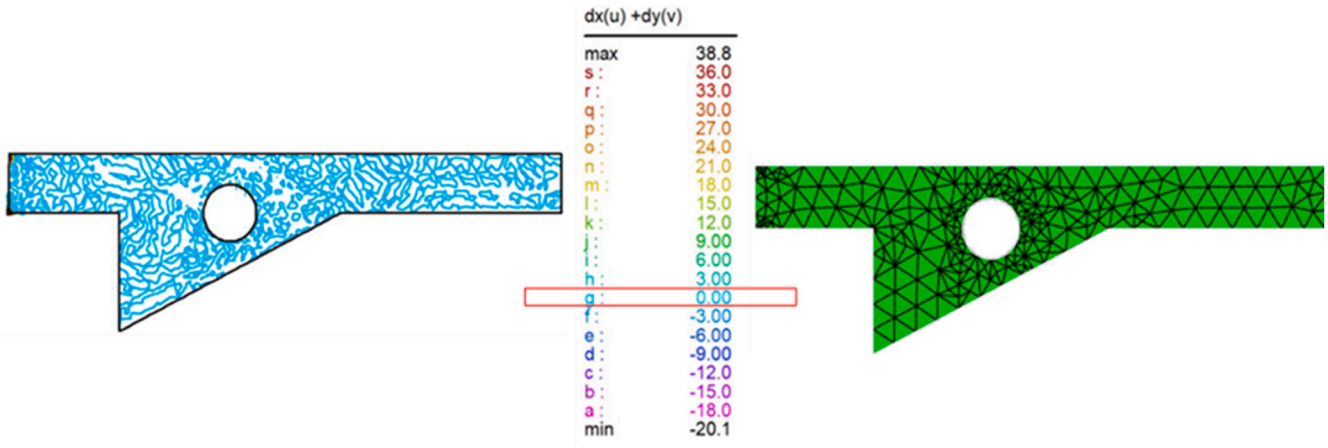

Fig. 2. Validation of continuity equation ($\partial U/\partial X + \partial V/\partial Y$).

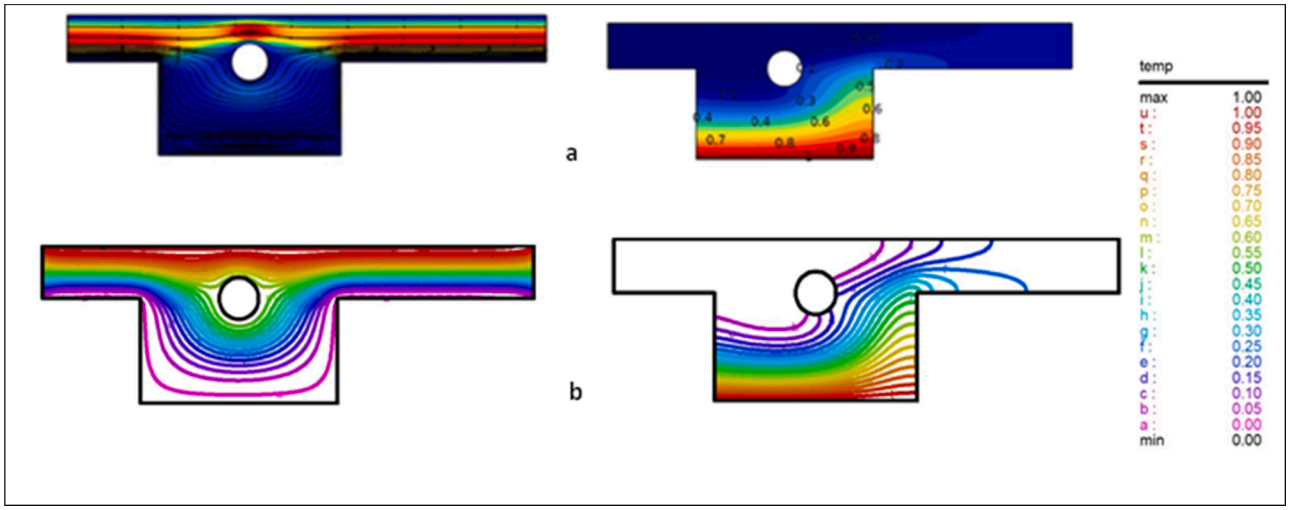

Fig. 3. Isotherms and streamlines comparisons at Ω = 0, Ri= 1, φ = 0.02, α = 0, R = 0.1, Pr = 6.2, Re = 10, a) Qureshi et al. [32], b) present study.

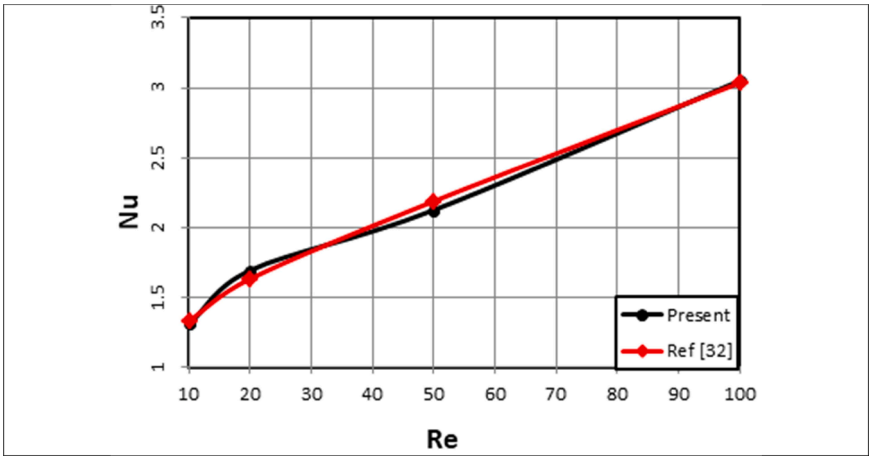

Fig. 4. Nusselt number comparison a) present study; b) Ri = 1, Pr= 6.2, R = 0.1, Ω = 0, φ = 0.02 [32].

minimum network size at which the Nusselt number stabilizes.

Five distinct grid densities were investigated to fine-tune the results and assess the accuracy of the numerical procedure. The relative inaccuracy and the difference in the average Nusselt number (Nu) for the hot surface are explained in Fig. 6. Interestingly, the findings show that the average Nu values match closely when the left wall and inclined wall are both heated, with relative errors remaining between 10^{-4} and 10^{-6}. An error tolerance of 10^{-4} was chosen as the compromise for result accuracy, guaranteeing a fair evaluation of accuracy and computational efficiency.

Table 2
Nusselt number comparison with ref [32].
For Ri= 1, Pr= 3.6, R = 0.1, Ω = 0 and φ = 0.02.

Re	Present work Nu	Qureshi et al. [32] Nu	Error
10	1.307	1.329	1.65 %
20	1.693	1.632	3.60 %
50	2.124	2.187	2.88 %
100	3.07	3.035	1.14 %

Table 3
Sensitivity test of grid at Ri = 1, Pr= 6.2, Re = 5, Ω = 5 and φ = 0.02.

Nodes (Cells)	471 (201)	610 (264)	6424 (3088)	20,908 (10,174)	72,446 (35,574)
Nu_{av}	2.188932	2.425984	3.602124	3.778520	3.902238
Time (*sec*)	7	15	485	5789	24,500

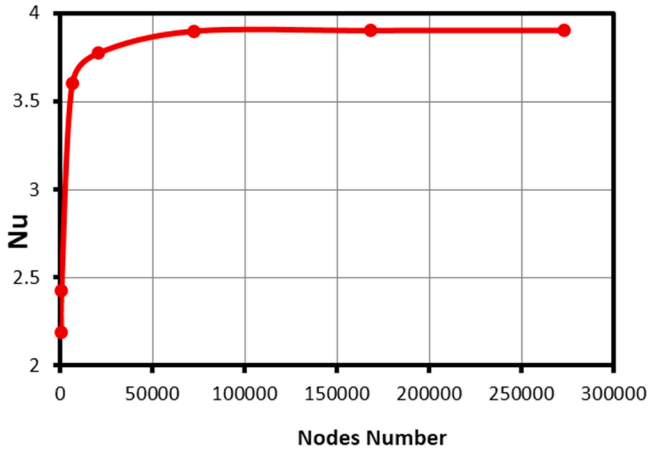

Fig. 5. Mesh independence study for Ri = 1, Pr= 6.2, Re = 5, Ω = 5 and φ = 0.02.

Fig. 7 shows the cross section of the network at a spacing mesh Sm= $2*(X^2 + Y^2) = 0.1$, it can be seen that the mesh is un uniformally distrbution while Fig .7b represents the mash at a spaing mesh Sm = 0.07 and we notce that the mesh distribution is uniform and reliable.

3.3. Solution method and generation of the mesh

We utilized the Galerkin finite element method to solve the governing equations encompassing continuity, momentum, and energy within our study. The FlexPDE package is utilized for implementing the finite element method, we analyzed the laminar mixed convection and nanofluid motion occurring inside a square enclosure with a rotating cylinder. It becomes evident in the numerical simulation domain that this set of relations can exhibit high oscillations or even become indeterminate due to the inclusion of the pressure term in the momentum equations. To address this challenge, we employed the penalty FEM method, wherein the pressure (P) is removed using a penalty parameter (λ) to enforce incompressibility. Fig. 8 illustrates the flowchart outlining the application of the FEM to solve the governing equations using the FlexPDE package.

The method employed to regulate cell density in the generated mesh by FlexPDE in the current study is known as implicit density. In this approach, the mesh cell density conforms to the spacing of points along the bounding segments. Consequently, a very small segment in the boundary will result in a region of small cells surrounding the segment.

Once the initial mesh is established, FlexPDE continuously assesses the solution error and refines the mesh as needed to achieve the desired accuracy. In time-dependent problems, an adaptive refinement process is also applied to the initial values of the variables to adjust the mesh in regions where variables experience rapid changes. However, it's worth noting that cells generated by this adaptive refinement process can be incorporated later on, whereas cells created by the initial explicit density controls are fixed and cannot be refined.

4. Results and discussions

The primary objective of the current investigation is to comprehensively examine and comprehend the influences of crucial governing parameters of heat transfer within a distinct system. This system comprises a horizontal channel featuring a triangular-shaped cavity affixed to the bottom wall, filled with an Ag-MgO-water hybrid nanofluid, and incorporating an adiabatic rotational cylinder. The study systematically delves into the effects of critical factors such as Re number, rotation speed of the cylinder (Ω), horizontal location of the cylindrical obstacle (Xo), and the positioning of the hot wall. In this study, we examine the influence of hybrid nanofluid on the flow characteristics and thermal field of mixed convection heat transfer in an open channel.

The numerical results provide a clear picture and a thorough comprehension of the process controlling streamline and isotherm distribution in the system under investigation. The results also systematically explain the average Nusselt number (Nu) along the heated wall. Employing the graphical display of streamlines and isotherms, the research offers significant insights into the temperature distributions and fluid flow patterns, enabling a comprehensive understanding of the complex dynamics associated with mixed convection in the given configuration. The average Nusselt number is systematically analyzed to

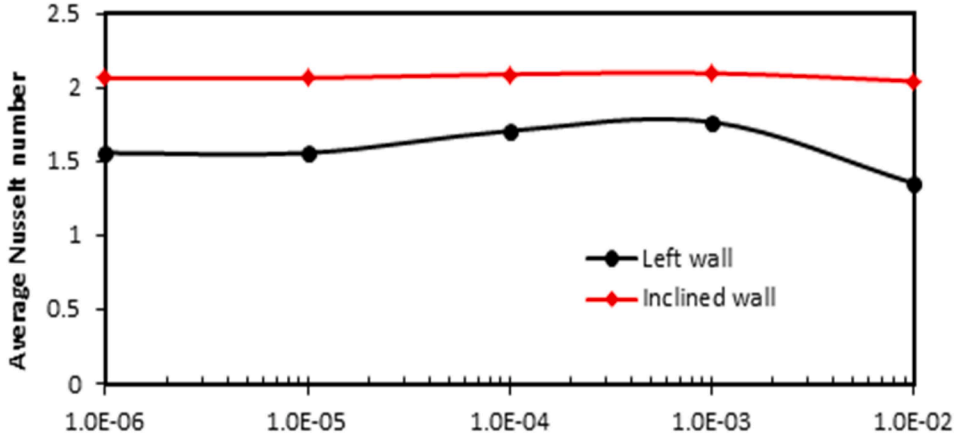

Fig. 6. Dependency Nu number on the imposed accuracyfor Ω = 5, Ri = 1, Re = 10, Xo = 1, and Yo = 0.5.

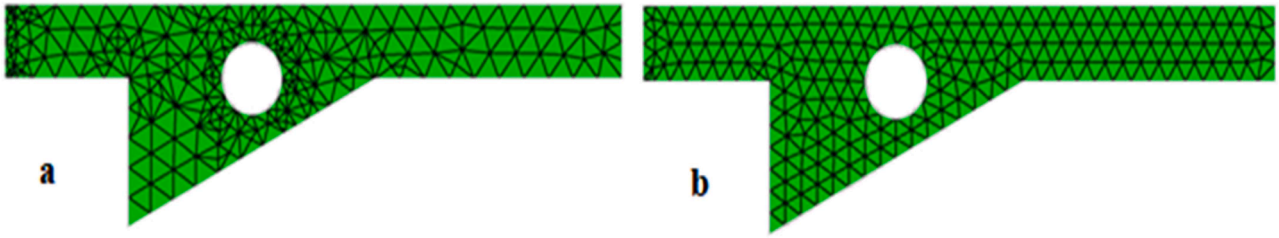

Fig. 7. Mesh's cross section for different specing mesh a) Sm = 0.1 b) Sm = 0.07.

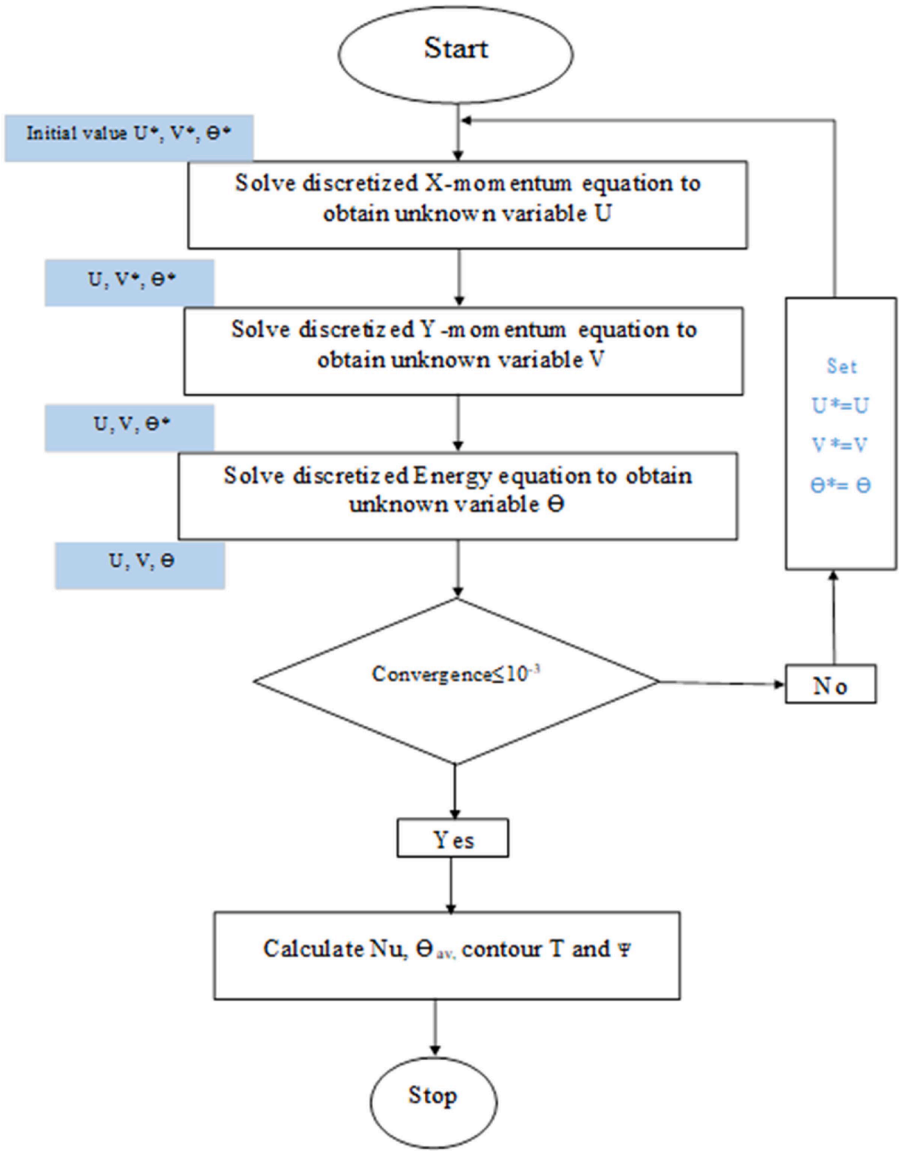

Fig. 8. Floew chart of numerical solution by FlexPDE package.

provide a more thorough understanding of the thermal behavior of the system under study and to aid in the quantitative evaluation of its heat transfer properties.

4.1. Flow and thermal fields characteristics

4.1.1. Effects of Reynolds number, (Re)

Regarding fluid dynamics, heat transmission is greatly influenced by the Reynolds number (Re), which has a noticeable effect on flow properties as Re rises. Considering the two scenarios and cases examined in this study, one where the triangular cavity's inclined wall is heated and another where the cavity's left wall is heated Fig. 9 displays streamlines and isotherms for two different Reynolds values, Re = 10 and Re = 50. The remaining parameters are as follows: rotation rate (Ω = 5), the horizontal location of the cylindrical obstacle (Xo = 0.5), cylinder radius (R = 0.12), angle of magnetic field (α = 0), Richardson number (Ri = 1), Hartmann number (Ha = 25), Prandtl number (Pr = 6.2).

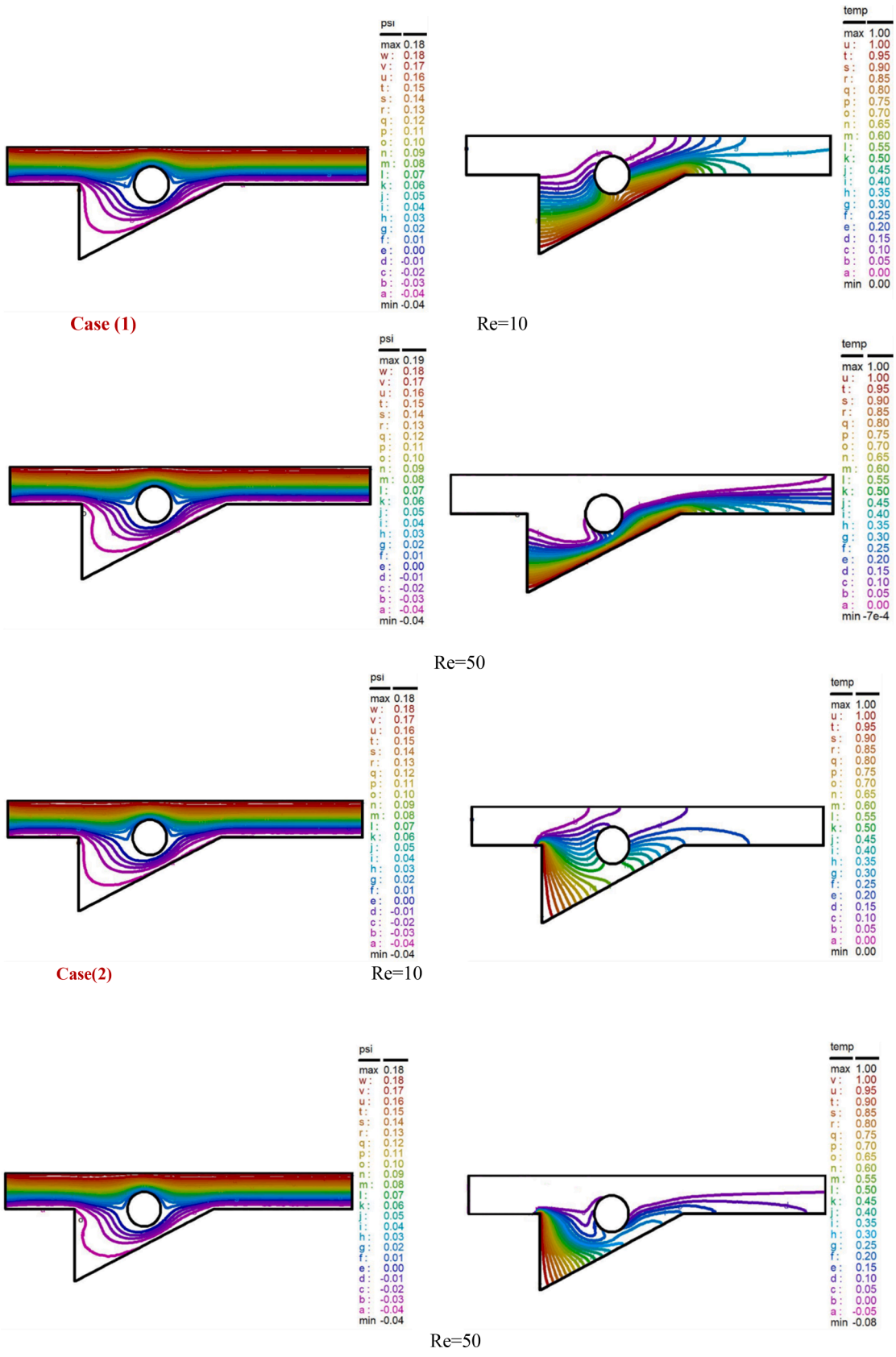

Fig. 9. Streamline (on the left) and isotherms (on the right) for different values of Reynolds number and two cases at $\varphi = 0.02$, $\alpha = 0$, $\Omega = 5$, $Yo = 0.5$.

The streamlines in the illustrated picture show a parallel flow in the channel, while the flow lines inside the cavity are curved, with the strongest streamlines close to the upper wall. Heat transfer increases with Reynolds number (Re), yet the flow behavior remains unchanged over the whole channel length. Interestingly, compared to the triangular cavity, the increase in heat transfer is more noticeable on the channel surface.

In terms of isotherms, the first case shows stratified lines near the heated surface at low Reynolds numbers (Re = 10), indicating diffusion-dominated heat transfer. Denser isotherm lines emerge along the heated wall as the Reynolds number (Re = 50) rises, indicating a greater impact of convective currents and a reduction in the thermal boundary layer. In the second scenario, where the triangle cavity's left wall is heated, isothermal lines at Re = 10 resemble a conduction-like distribution and are almost parallel to the hot wall and the inner cylinder. The isothermal lines along the hot wall get denser at Re = 50, indicating the increased influence of convective currents, a reduction in the thermal boundary layer, and an increase in the heat transfer rate.

4.1.2. Effect of the direction of cylinder rotation

Heat transmission dynamics are found to be significantly influenced by cylinder rotation. The effects of cylinder rotation direction on flow and temperature fields are explained in Figs.10 and 11, which consider different rotation speeds for both clockwise rotations. The Hartmann number (Ha) = 25, the cylinder radius (R) = 0.12, the Prandtl number (Pr) = 6.2, the horizontal placement of the cylindrical obstruction (Yo) = 0.5, the Richardson number (Ri) = 1, and the Reynolds number (Re) = 10 are the circumstances for which the simulations are run.

In Fig. 10, the inclined wall is subjected to heating, while the cylinder positioned at the center of the enclosure rotates both clockwise and counterclockwise. Recirculating cells are created between the convective flow and the cylinder by the motion of the revolving cylinder. In the case of Ω = 25 and Ω = -25, the streamlines create a sizable vortex encompassing the whole interior of the triangular cavity, especially the area surrounding the solid cylinder. On the other hand, there is no vortex appears in the corner of the triangular cavity for Ω = -5 and 5. The figure, i.e., Ω = -5 and 5, clearly shows an increase in flow strength for smaller cylinder rotation values. The elevated temperature within the cavity is attributed to the fixed temperature condition (θ= 1) enforced on the inclined cavity wall. Isotherms indicate uniform heat distribution throughout the enclosure, leading to an enhanced heat transfer rate in the inclined position. In Fig. 11, where the left wall is heated, and the cylinder at the enclosure's center rotates both clockwise and counterclockwise, it is observed that the flow field trend mirrors that of Fig. 10. Moreover, the distribution of isotherms within the cavity results in an increased heat transfer rate at the left position.

4.2. Heat transfer characteristics

4.2.1. Effect of the direction of cylinder rotation

An important factor to consider while studying mixed convection in an enclosure is how an inner circular cylinder's direction of rotation affects the heat transfer rate along the heated wall. This paper investigates how changes in the Reynolds number (Re) and cylinder rotation direction affect the average Nusselt number (Nu). Fig.12 shows the relationship between average Nu and Re for the inclined hot wall (case one) of the triangular hollow, considering the inner cylinder's two rotation directions (clockwise and counterclockwise) and its various rotating speeds. The results show that at all rotational speeds, the Nu number increases linearly with increasing Reynolds number; higher values are seen when the inner cylinder rotates counterclockwise. This result was obtained by finding that the direction of the buoyant force is aligned with a decrease in thermal boundary layer thickness resulting from an increase in counterclockwise rotational speed. This alignment improves the process of heat exchange.

Fig. 13 shows the effect of the inner cylinder rotation direction for case two, where the left wall of the triangular cavity is heated. For stationary, clockwise, and counterclockwise rotation cases, the Nu number is displayed as a function of Re. This analysis is carried out for the given parameters (φ = 0.02, α = 0, R = 0.12, Ha = 25, Pr = 6.2, Xo = 1, and Yo = 0.5).

The figure demonstrates that irrespective of angular velocities, the response to Reynolds number variations remains consistent across all ranges of cylinder rotation. Initially, there is a rise in Nusselt values within the range of 10 ≤ Re ≤ 50. Notably, the Nusselt numbers are higher for counterclockwise flow compared to those for clockwise flow. Subsequently, a decline in the Nusselt number is observed within the range of 50 ≤ Re ≤ 100, with higher values observed when the flow direction is clockwise.

These observations can be explained physically by comprehending the intricate interplay between buoyancy forces and rotational effects. The counterclockwise rotation promotes more effective heat exchange by increasing the convective currents and decreasing the thickness of the thermal barrier layer. These discoveries provide essential implications to advance our understanding of how directional rotation affects heat transport in mixed convective heat transfer.

4.2.2. Effect of the location of inner cylinder rotation

To obtain a more profound understanding of the flow dynamics, Figs. 14 and 15 for both scenarios examine the impact of the spinning cylinder's horizontal location (Xo) on the average Nusselt number (Nu), taking into consideration particular Reynolds numbers (Re= 10, 30, 50, and 100). Nu shows a similar pattern for all Reynolds number ranges throughout various values of Xo; for case one, as shown in Fig.14, with an increase for (0.65 ≤ Xo ≤ 0.9) and a drop for (0.9 < Xo ≤ 1). Nu values are optimal when Xo= 0.9 because the flow direction aligns with the buoyancy force and the least amount of fluid obstruction force.

The association between the average Nu number at the left heated wall and the distance Xo is shown in Fig. 15. It is clear that the average Nu number grows substantially for all Reynolds number values within a particular range (0.65 < Xo ≤ 0.75). At higher Reynolds numbers, higher Nu values are seen, and at Xo= 0.75, maximal performance is reached. Lower obstruction forces come from the alignment of the buoyancy force direction with the flow direction, which explains this phenomenon. On the other hand, for all Reynolds number values within the range (0.75 < Xo ≤ 1), an increase in the distance between the starting point of the channel and the center of the spinning cylinder (Xo) results in a drop in the average Nu number. This finding emphasizes the intricate relationship between Xo, Reynolds number, and heat transfer properties in the studied configuration.

4.2.3. Effect of cylinder rotation speed

The study presents the influence of cylinder rotation speed on mixed convection flow in a horizontal channel with an open-top cavity attached to the bottom channel wall. The Nusselt number (Nu) at the hot wall is plotted versus the Re number. The analysis is performed for clockwise and counterclockwise rotations of the inner cylinder, as shown in Figs. 16 and 17, respectively. The analysis considers parameters such as φ = 0.02, α = 0, R = 0.12, Ha = 25, Pr = 6.2, Xo = 1, and Yo = 0.5. The data indicates that the Nu values consistently demonstrate a predictable pattern in response to changes in Re for various cylinder rotation speeds and clockwise and counterclockwise directions. The findings demonstrate that the Nusselt number significantly escalates as the cylinder rotation speed increases, especially when the cylinder rotates clockwise.

The observed behavior indicates a direct relationship between the speed at which the inner cylinder rotates and increased heat transmission. This highlights the significance of the rotational dynamics in altering the thermal properties of the system. In the clockwise flow depicted in Fig. 16, there is a noticeable rise in Nusselt values as the angular velocity increases within the range of 10 ≤ Re ≤ 30, whereas the opposite trend is observed within the range of 50 ≤ Re ≤ 100. This

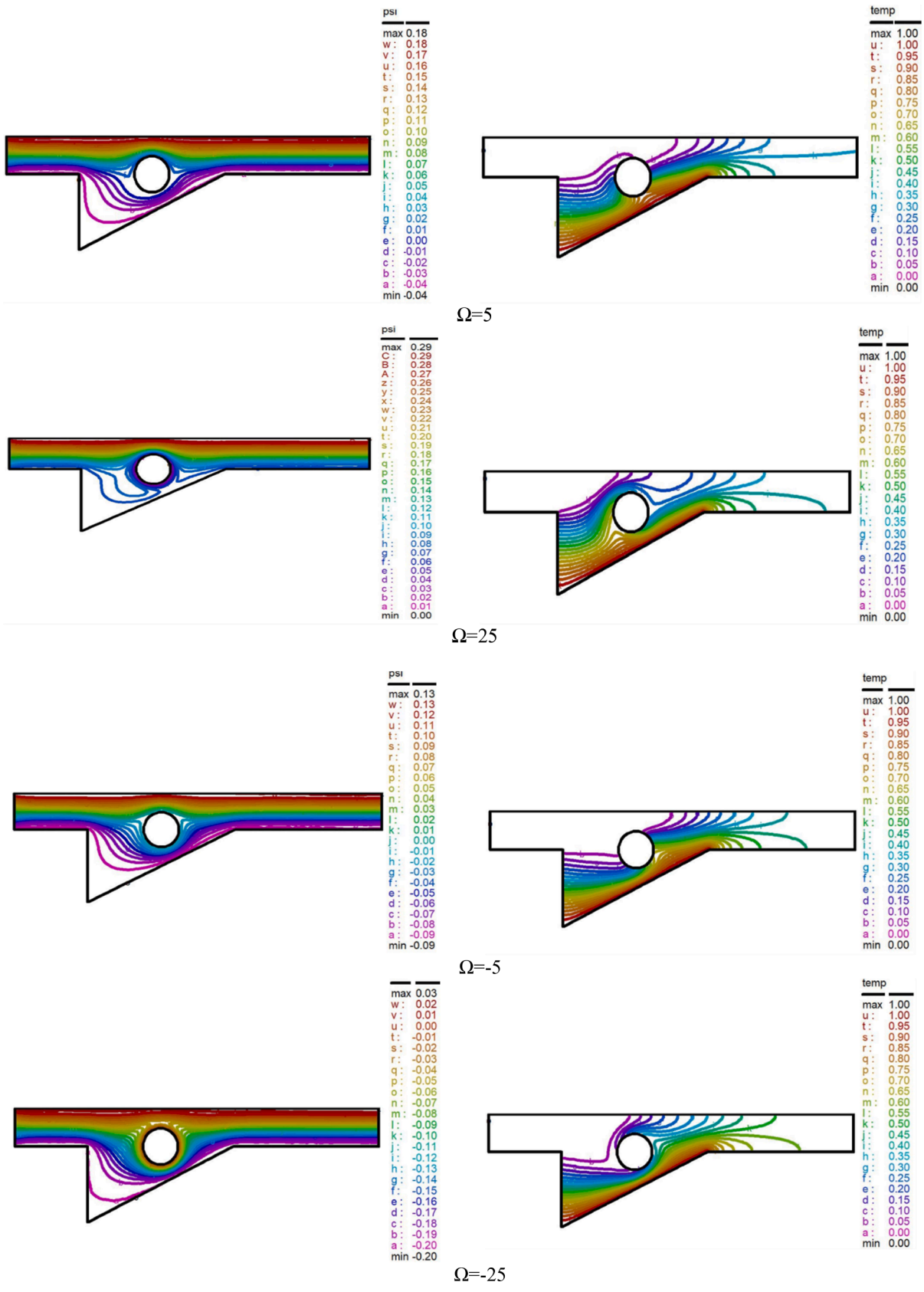

Fig. 10. Streamlins (on the left) and Isotherms(on the right)for inclined wall heated case at $\varphi = 0.02$, $\alpha = 0$, Yo = 0.5, Re = 10 and different values of cylinder rotation.

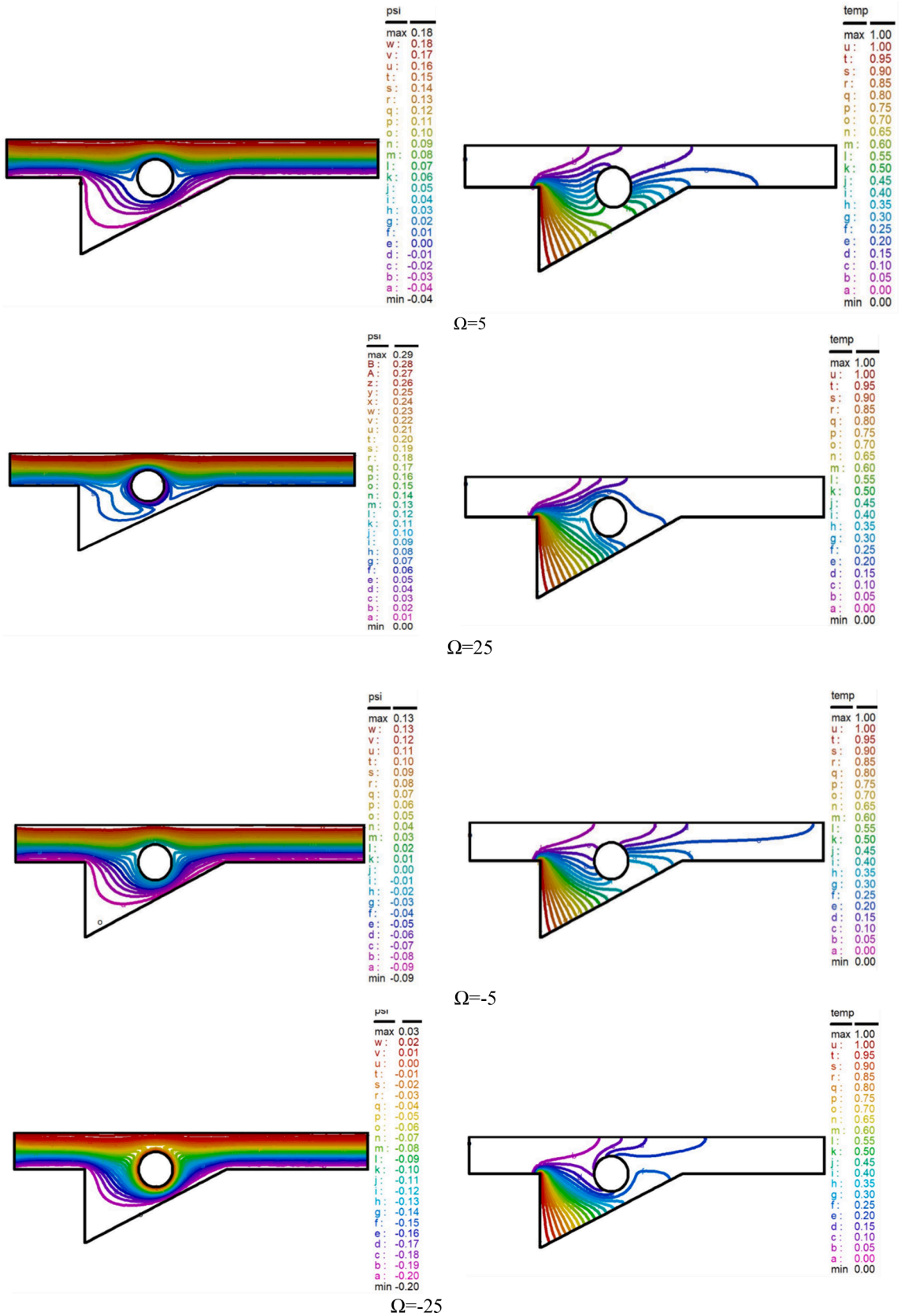

Fig. 11. Streamline (on the left) and Isotherms(on the right)for the left wall heated case at $\varphi = 0.02$, $\alpha = 0$, Yo = 0.5, Re = 10, and different values of cylinder rotation.

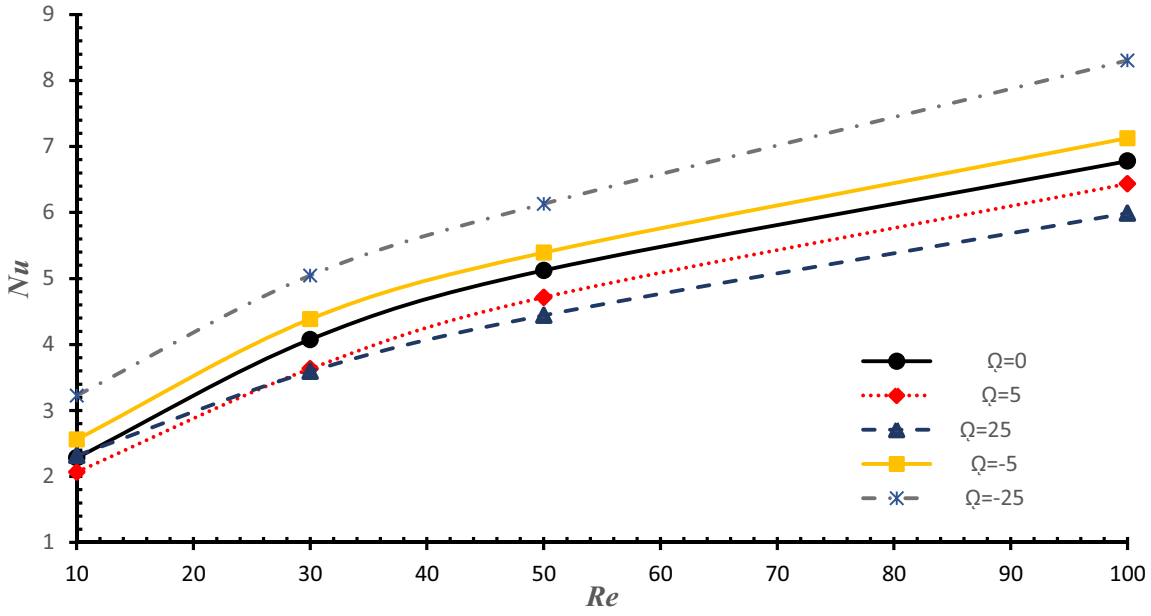

Fig. 12. Effect of the direction of cylinder rotation on the average Nu number for the heated inclined wall at $\varphi = 0.02$, $\alpha = 0$, $X_o = 1$, $Y_o = 0.5$.

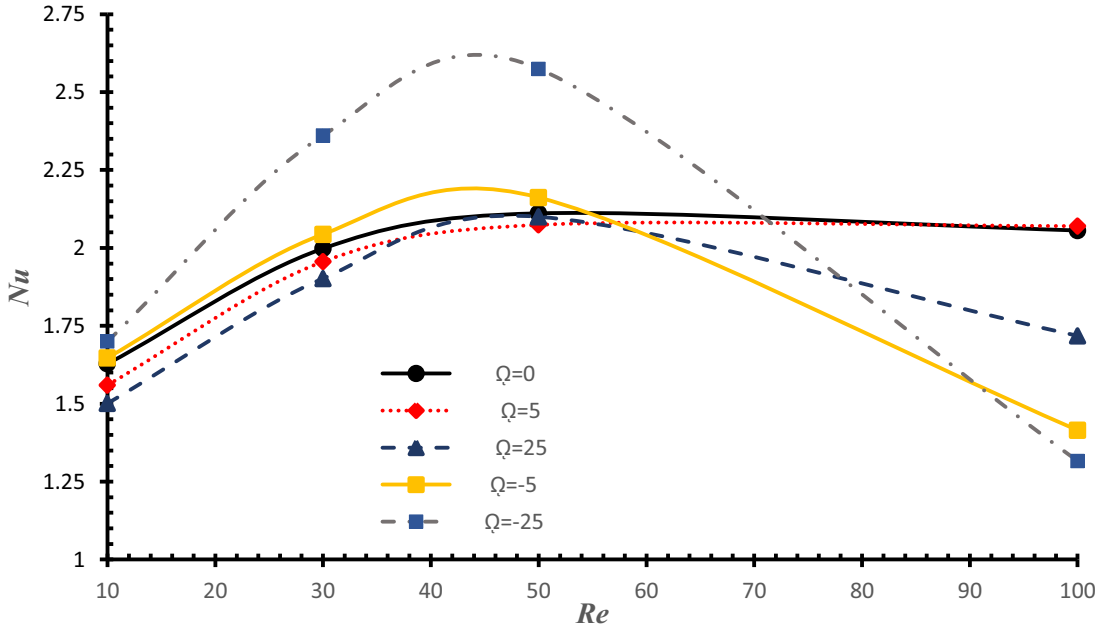

Fig. 13. Effect of the direction of cylinder rotation on the average Nu number for the heated left wall at $\varphi = 0.02$, $Ri = 1$, $X_o = 1$, $Y_o = 0.5$.

phenomenon is attributed to the higher Nusselt numbers at lower angular velocities, wherein the isotherms indicate enhanced heat distribution within the cavity, consequently resulting in an augmented heat transfer rate. Fig. 17 illustrates an increase in Nusselt number with the augmentation of counterclockwise flow. The counterclockwise rotation fosters heat exchange by amplifying convective currents and reducing the thickness of the thermal boundary layer.

5. Conclusions

Mixed convection and heat transfer within cavities represent a significant phenomenon with implications in both scientific and engineering domains. This study investigates mixed convection within a horizontal channel containing a rotating cylinder in a triangular cavity using a finite element approach (FlexPDE). Key parameters (Re, Ri, cylinder location) were varied to assess their impact on heat transfer. Two scenarios of combined natural and forced convection are investigated: In Case 1, all channel walls, the left wall of the cavity, and the surface of the rotating cylinder are adiabatic, while the inclined wall of the cavity is isothermal. In Case 2, all channel walls, the right wall of the cavity, and the surface of the rotating cylinder are adiabatic, except for the left wall of the cavity, which is isothermal.

The Results showed that increasing Re enhances the Nusselt number (Nu), indicating improved efficiency and the higher angular velocity also correlates with increased Nu, highlighting its role in heat transfer. Observed trends in Nu emphasize the importance of Re, rotation speed, location, and Ri for optimizing heat transfer in similar systems, guiding future research.

Future work may include investigating diverse nanofluid

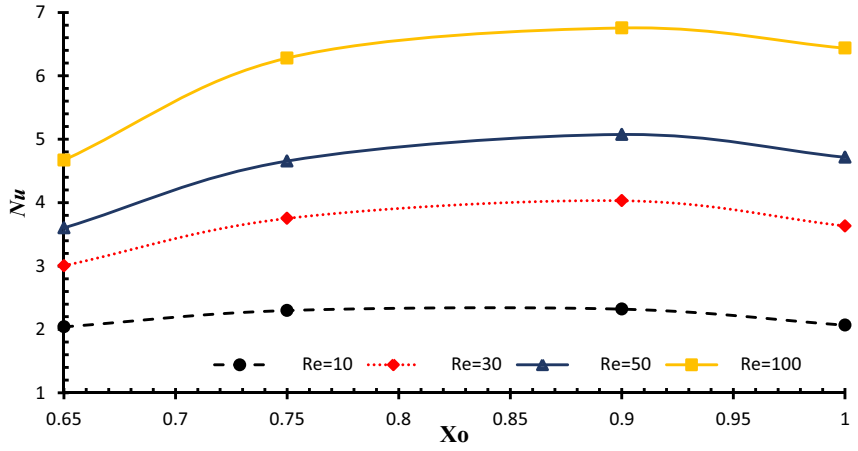

Fig. 14. Variation of the average Nu number with the location of the cylinder for the heated inclined wall at Ri = 1, Xo= 1 Y_o = 0.5 and Ω= 5.

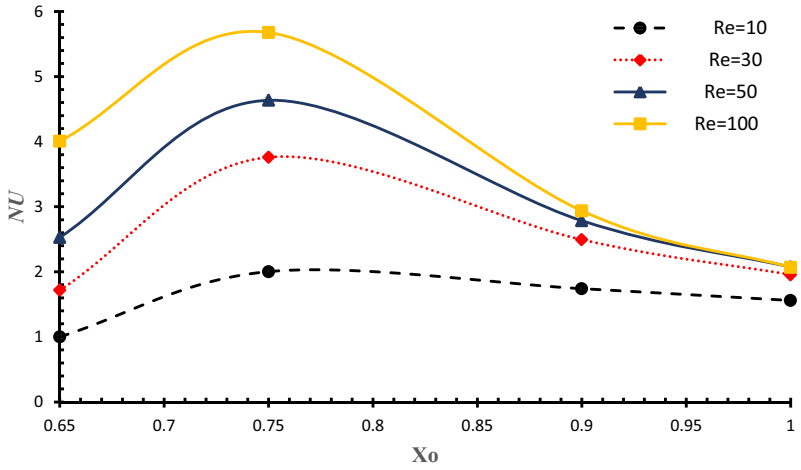

Fig. 15. Variation of the average Nu number with the location of the cylinder for a left heated wall at Ri = 1, Xo= 1 Y_o = 0.5 and Ω= 5.

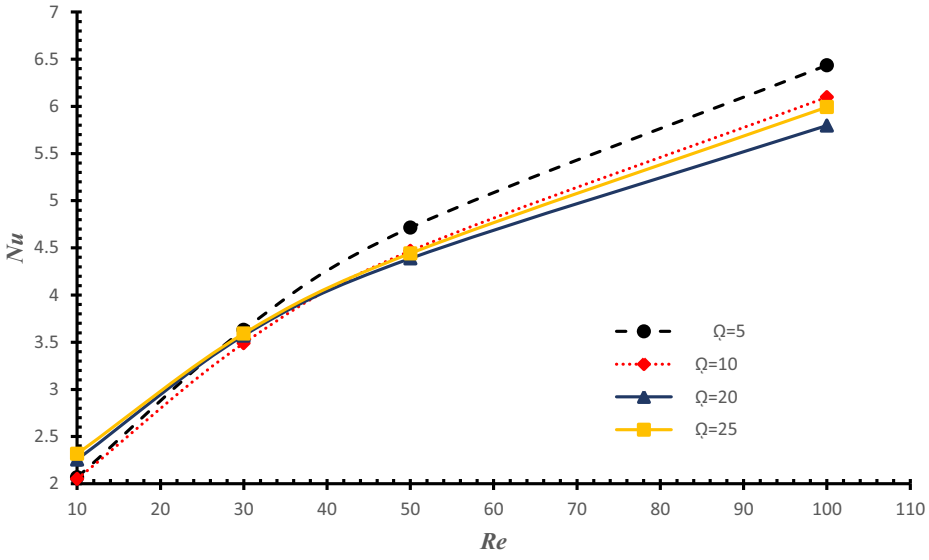

Fig. 16. Variation of the Nu with Re for heated inclined wall and with clockwise cylinder direction at Ri = 1, Pr = 6.2, X_o= 1, Y_o = 0.5.

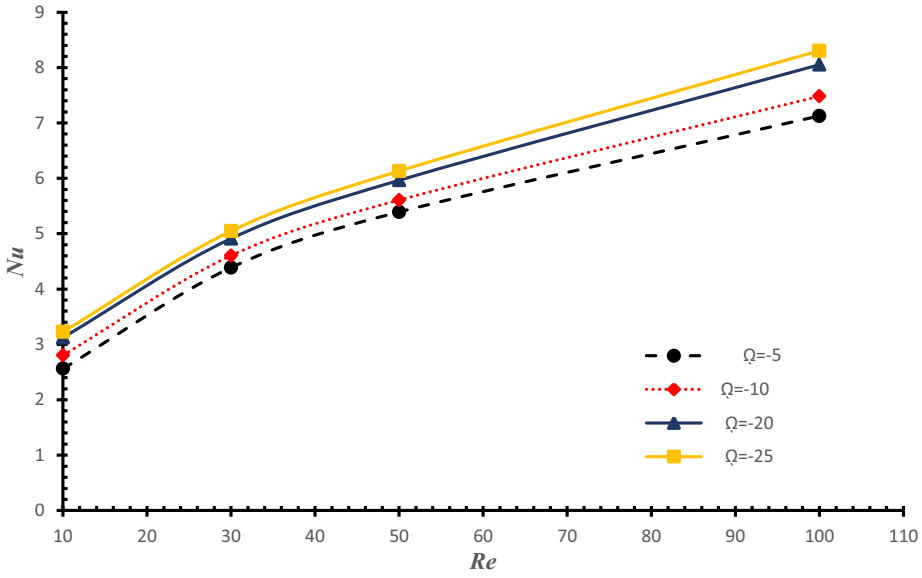

Fig. 17. Variation of the Nu with Re for inclined wall and with counterclockwise cylinder direction at Ri = 1, X_o= 1, Y_o = 0.5.

compositions, exploring additional geometrical parameters, extending to three-dimensional simulations, considering external factors like magnetic fields, and exploring optimization techniques for practical applications.

CRediT authorship contribution statement

Falah A. Abood: Methodology, Data curation. **Zainab K. Radhi:** Visualization, Resources, Formal analysis. **Ali K. Hadi:** Writing – original draft, Methodology, Investigation. **Raad Z. Homod:** Software, Conceptualization. **Hayder I. Mohammed:** Writing – original draft, Supervision, Investigation.

Declaration of competing interest

The authors declare that they have no known competing financial interests or personal relationships that could have appeared to influence the work reported in this paper.

Data availability

No data was used for the research described in the article.

References

[1] F.A. Abood, S.J. Yaseen, I.G. Mohammed, R.Z. Homod, H.I. Mohammed, Enhancing thermal performance in a magnetized square cavity: novel insights from mixed convection of Ag-MgO nanofluid around a rotating cylinder, Int. J. Thermofluids 22 (2024) 100630, https://doi.org/10.1016/j.ijft.2024.100630.

[2] M.A. Alomari, K. Al-Farhany, Q.H. Al-Salami, I. Ali, N. Biswas, M.H. Mohamed, F. Alqurashi, Numerical analysis to investigate the effect of a porous block on MHD mixed convection in a split lid-driven cavity with nanofluid, Int. J. Thermofluids 22 (2024) 100621, https://doi.org/10.1016/j.ijft.2024.100621.

[3] R.Z. Homod, F.A. Abood, S.M. Shrama, A.K. Alshara, Empirical correlations for mixed convection heat transfer through a fin array based on various orientations, Int. J. Therm. Sci. 137 (2019) 627–639.

[4] K.M. Sahari, M.A. Jalal, R.Z. Homod, Y.K. Eng, Dynamic indoor thermal comfort model identification based on neural computing PMV index, in: IOP Conference Series: Earth and Environmental Science 16, IOP Publishing, 2013 012113.

[5] A. Almssad, A. Almusaed, R.Z. Homod, Masonry in the context of sustainable buildings: a review of the brick role in architecture, Sustainability. 14 (22) (2022) 14734.

[6] K. Suchana, M.M. Islam, M.M. Molla, Lattice Boltzmann simulation of cross diffusion via Soret and Dufour effects on natural convection of experimental data based MWCNTs-H2O nanofluids in an ʟ-shaped enclosure, Int. J. Thermofluids 21 (2024) 100546, https://doi.org/10.1016/j.ijft.2023.100546.

[7] K.S. Al Kalbani, M. Rahman, M. Ziad Saghir, Entropy generation in hydromagnetic nanofluids flow inside a tilted square enclosure under local thermal nonequilibrium condition, Int. J. Thermofluids 5-6 (2020) 100031, https://doi.org/10.1016/j.ijft.2020.100031.

[8] H. Saleh, R. Roslan, I. Hashim, Natural convection heat transfer in a nanofluid-filled trapezoidal enclosure, Int. J. Heat Mass Transf. 54 (2011) 194–201.

[9] A.A. Abbasian, G.A. Sheikhzadeh, R. Heidary, N. Hajialigol, M.E. Qomi, Numerical study of mixed convection in a lid-driven enclosure with a centered body using nanofluid variable properties, JUS 2 (2012) 51–60.

[10] M. Mahmoodi, S.M. Hashemi, Numerical study of natural convection of a nanofluid in C-shaped enclosures, Int. J. Therm. Sci. 55 (2012) 76–89.

[11] S. Izadi, T. Armaghani, R. Ghasemiasl, A.J. Chamkha, M. Molana, A comprehensive review on mixed convection of nanofluids in various shapes of enclosures, Powder Technol. 343 (2019) 880–907.

[12] C. UYSAL, M.E. KORKMAZ, Estimation of entropy generation for Ag-MgO/water hybrid nanofluid flow through rectangular minichannel by using artificial neural network, J. Polytech. 22 (1) (2019) 41–51.

[13] M. Hasan, A. Azad, R. Hossain, M. Rahman, M. Karim, Analysis of mixed convection under radiation and magnetohydrodynamics utilizing Kerosene-CNT nanofluid in a lid-driven cavity, Int. J. Thermofluids 21 (2024) 100528, https://doi.org/10.1016/j.ijft.2023.100528.

[14] S. Hussain, M.A. Qureshi, S.E. Ahmed, Impact of wavy porous layer on the hydrodynamic forces and heat transfer of hybrid nanofluid flow in a channel with cavity under the effect of partial magnetic field, J. Non-Equilib. Thermodyn. (2023) aop.

[15] I. Ahmadianfar, R.M. Noori, H. Togun, M.W. Falah, R.Z. Homod, M. Fu, B. Halder, R. Deo, Z.M. Yaseen, Multi-strategy Slime Mould Algorithm for hydropower multi-reservoir systems optimization, Knowl. Based Syst. 250 (2022) 109048.

[16] A.J. Chamkha, F. Selimefendigil, Forced convection of pulsating nanofluid flow over a backward facing step with various particle shapes, Energies (Basel) 11 (2018).

[17] S. Lee, S.U. Choi, S. Li, J.A. Eastman, Measuring thermal conductivity of fluids containing oxide nanoparticles, ASME. J. Heat Transfer. 121 (2) (1999) 280–289, https://doi.org/10.1115/1.2825978.

[18] K. Khanafer, K. Vafai, M. Lightstone, Buoyancy driven heat transfer enhancement in a two-dimensional enclosure utilizing nanofluids, Int. J. Heat Mass Transf. 46 (2003) 3639–3653.

[19] M.M. Ali, R. Akhter, M. Alim, Hydromagnetic mixed convection in a triangular shed filled by nanofluid and equipped with rectangular heater and rotating cylinders, Int. J. Thermofluids 11 (2021) 100105, https://doi.org/10.1016/j.ijft.2021.100105.

[20] A.K. Santra, S. S, N. Chakraborty, Study of heat transfer in a differentially heated square cavity using copper-water nanofluid, Int. J. Therm. Sci. 48 (2008) 1113–1122.

[21] B. El hadoui, M. Kaddiri, Aspect ratio's critical role in enhancing natural convective heat transfer with temperature-dependent nanofluids within rectangular enclosures, Int. J. Thermofluids 20 (2023) 100501, https://doi.org/10.1016/j.ijft.2023.100501.

[22] M.S. Islam, S. Islam, M.N.A.A. Siddiki, Numerical simulation with sensitivity analysis of MHD natural convection using Cu-TiO2-H2O hybrid nanofluids, Int. J. Thermofluids 20 (2023) 100509, https://doi.org/10.1016/j.ijft.2023.100509.

[23] Y. Gao, I.M. Shigidi, M.A. Ali, R.Z. Homod, M.R. Safaei, Thermophysical properties prediction of carbon-based nano-enhanced phase change material's using various machine learning methods, J. Taiwan. Inst. Chem. Eng. (2023) 104662.

[24] A. Almusaed, A. Almssad, I. Yitmen, R.Z. Homod, Enhancing student engagement: harnessing "AIED"'s power in hybrid education—a review analysis, Educ. Sci. (Basel) 13 (7) (2023) 632, https://doi.org/10.3390/educsci13070632.
[25] R.Z. Homod, H. Togun, A.K. Hussein, F.N. Al-Mousawi, Z.M. Yaseen, W. Al-Kouz, H.J. Abd, O.A. Alawi, M. Goodarzi, O.A. Hussein, Dynamics analysis of a novel hybrid deep clustering for unsupervised learning by reinforcement of multi-agent to energy saving in intelligent buildings, Appl. Energy 313 (2022) 118863.
[26] H.E. Patel, T. Pradeep, T. Sundararajan, A. Dasgupta, N. Dasgupta, S.K. Das, A micro-convection model for thermal conductivity of nanofluid, Pramana-J. Phys. 65 (2005) 863–869.
[27] A. Saha, A. Chakravarty, K. Ghosh, N. Biswas, N.K. Manna, Role of obstructing block on enhanced heat transfer in a concentric annulus, in: Waves *Random and Complex Media*, 2022, pp. 1–25. https://doi.org/10.1080/17455030.2022.2106386.
[28] A. Saha, N.K. Manna, K. Ghosh, et al., Analysis of geometrical shape impact on thermal management of practical fluids using square and circular cavities, Eur. Phys. J. Special Top. 231 (3) (2022) 2509–2537.
[29] N. Biswas, D.K. Mandal, N.K. Manna, et al., Magneto-hydrothermal triple-convection in a W-shaped porous cavity containing oxytactic bacteria, Sci. Rep. 12 (2022) 18053.
[30] D.K. Mandal, N. Biswas, NK. Manna, D.K. Gayen, R.S.R. Gorla, AJ. Chamkha, Thermo-fluidic transport process in a novel M-shaped cavity packed with non-Darcian porous medium and hybrid nanofluid: application of artificial neural network (ANN), Phys. Fluids 34 (3) (2022).
[31] N.K. Manna, N. Biswas, D.K. Mandal, U.K. Sarkar, H.F. Öztop, N. Abu-Hamdeh, Impacts of heater-cooler position and Lorentz force on heat transfer and entropy generation of hybrid nanofluid convection in quarter-circular cavity, Int. J. Numer. Methods Heat. Fluid. Flow. 33 (3) (2023) 1249–1286.
[32] M.A. Qureshi, S. Hussain, M.A. Sadiq, Numerical simulations of MHD mixed convection of hybrid nanofluid flow in a horizontal channel with cavity: impact on heat transfer and hydrodynamic forces, Case Stud. Therm. Eng. 27 (2021) 101321.
[33] M. Ghalambaz, A. Doostani, E. Izadpanahi, A.J. Chamkha, Conjugate natural convection flow of Ag-MgO/water hybrid nanofluid in a square cavity, J. Therm. Anal. Calorim 139 (2020) 2321–2336.
[34] M. Hemmat Este, A.A.A Arani, M. Rezaie, W.M. Yan, A. Karimipour, Experimental determination of thermal conductivity and dynamic viscosity of Ag-MgO/water hybrid nanofluid, Int. Commun. Heat Mass Tran. 66 (2015) 189–195.
[35] F. Selimefendigil, H.F. Oztop, Impact of a rotating cone on forced convection of Ag-MgAO/water hybrid nanofluid in a 3D multiple vented T-shaped cavity considering magnetic field effects, J. Therm. Anal. Calorim. 143 (2021) 1485–1501.
[36] H.P. Langtangen, K.A. Mardal, R. Winther, Numerical methods for incompressible viscous flow, Adv. Water Resour. 25 (2002) 1125–1146.
[37] Falah, et al., Inclination angle effects on heat transfer in a semi-circular enclosure, J. Appl. Sci. Eng. 26 (11) (2023) 1667–1676.